Article

Sensitivity of the Land–Atmosphere Coupling to Soil Moisture Anomalies during the Warm Season in China and its Surrounding Areas

Lan Wang [1], Shuwen Zhang [1,*], Xinyang Yan [2] and Chentao He [1]

[1] College of Atmospheric Sciences, Lanzhou University, No. 222 Tianshui South Road, Chengguan District, Lanzhou 730000, China; wangl20@lzu.edu.cn (L.W.); hecht2023@lzu.edu.cn (C.H.)
[2] Meteorological Service Center of Gansu Province, Lanzhou 730020, China; yanxy18@lzu.edu.cn
* Correspondence: zhangsw@lzu.edu.cn

Abstract: Significant temporal and spatial variability in soil moisture (SM) is observed during the warm season in China and its surrounding regions. Because of the existence of two different evapotranspiration regimes, i.e., soil moisture-limited and energy-limited, averaging the land–atmosphere (L–A) coupling strength for all soil wetness scenarios may result in the loss of coupling signals. This study examines the daytime-only L–A interactions under different soil moisture conditions, by using two-legged metrics in the warm season from May to September 1981–2020, partitioning the interactions between SM and latent heat flux (SM–LH, the land leg) from the interactions between latent heat flux and the lifting condensation level (LH–LCL, the atmospheric leg). The statistical results reveal large regional differences in warm-season daytime L–A feedback in China and its surrounding areas. As the soil becomes wetter, the positive SM–LH coupling strength increases in arid regions (e.g., northwest China, Hetao, and the Great Indian Desert) and the positive feedback shifts to the negative one in semi-arid/semi-humid regions (northeast and northern China). The negative LH–LCL coupling is most pronounced in wet soil months in arid regions, while the opposite is true for the Tibetan Plateau. In terms of intraseasonal variation, the large variability of SM in north China, the Tibetan Plateau, and India due to the influence of the summer monsoon leads to the sign change in the land segment coupling index, comparing pre- and post-monsoon periods. To further examine the impact of SM anomalies on L–A coupling and to explore evapotranspiration regimes in the North China Plain, four sets of sensitivity experiments with different soil moisture levels over a period of 10 years were conducted. Under relatively dry soil conditions, evapotranspiration is dominated by the soil moisture-limited regime with positive L–A coupling, regardless of external moisture inflow. The critical soil moisture value separating a soil moisture-limited and an energy-limited regime lies between 0.24 m^3/m^3 and 0.29 m^3/m^3. Stronger positive feedback under negative soil moisture anomalies may increase the risk of drought in the North China Plain.

Keywords: soil moisture; daytime-only mean land–atmosphere coupling; sensitivity experiment; evapotranspiration regime; drought

1. Introduction

Numerous studies have revealed that regional climate variability is partly due to the interactions between the land surface and the atmosphere and demonstrated the importance of land–atmosphere (L–A) coupling in shaping the development of weather and climate systems across various spatial and temporal scales [1]. Land–atmosphere coupling facilitates the daily circulation of clouds and precipitation, significantly influencing the water cycle [2,3]. At the daily time scale, L–A interactions affect the evolution of convective systems and precipitation triggering [4–6], as well as weather-scale atmospheric circulation [7,8]. It also contributes to the monsoon activity and regional climate on a seasonal scale [9]. In the context of global warming and worsening anthropogenic climate

change, the amplified L–A coupling will exacerbate the frequency and intensity of extreme events (e.g., extreme hot temperatures and heat weaves, compound soil and atmospheric drought, and floods) [10–15].

The "hot spots" of land–atmosphere coupling have been identified through observation and numerical modeling. The key regions appear to be unevenly distributed, mainly in transitional zones with semi-arid and semi-humid climates (e.g., the central Great Plains of North America, the Sahel, and northern India) [16–19]. Recent studies have indicated a trend of strong coupling zones shifting to non-transitional zones due to the increase in incoming shortwave radiation and the reduction in soil wetness [20,21]. Soil moisture (SM) is an important component of the global and regional energy and water balance. As a critical land surface variable, a great deal of work on L–A coupling is based on the effect of SM on the atmosphere or unusual changes in climate such as precipitation and temperature [16]. Based on the chain of physical processes, the whole process of L–A coupling is often split into several parts. The anomalies of SM affect evapotranspiration by partitioning incoming energy into latent and sensible heat fluxes, which in turn influence moisture and heat within the boundary layer, subsequently affecting precipitation [3,22]. In the absence of strong moisture advective effects, local evapotranspiration provides water vapor for precipitation and consumes most of the energy absorbed by the land surface. The latent heat flux affects low-level water vapor and moist static energy. For the positive feedback, when the soil is wet, the soil moisture evaporates due to the heating effect of solar radiation, leading to a decrease in the Bowen ratio (the ratio of sensible to latent heat flux) [17]. This will increase the low-level water vapor and moist static energy, thereby lowering the lifting condensation level (LCL). The negative feedback is influenced by a larger portion of the sensible heat flux, which affects the average temperature of the boundary layer. The increase in temperature leads to greater buoyancy generated by turbulent kinetic energy, resulting in a lower boundary layer [23]. For convective precipitation to form, the top of the planetary boundary layer (PBL) should exceed the LCL [24]. In general, moisture and temperature within the boundary layer collectively determine the LCL. Therefore, the evapotranspiration of the land surface plays a crucial role in the L–A coupling process.

Seneviratne et al. [3] discussed two evapotranspiration mechanisms and pointed out the existence of sensitivity intervals of SM. In regions dominated by the soil moisture-limited evapotranspiration regime, SM constrains the variability of evapotranspiration and the soil moisture–precipitation feedbacks are largely determined by the interactions between SM and evapotranspiration [19]. Under an energy-limited regime, evapotranspiration is independent of soil wetness, indicating that no significant L–A feedbacks occur. The statistical analysis of different climate conditions showed that in climatologically wet regions, the sensitivity of precipitation with respect to soil moisture is higher during dry months than in wet months and vice versa in climatologically dry regions [19]. Through the multiyear global land–atmosphere coupling experiment (GLACE), the coupling strength over areas with dry (wet) climate is enhanced during wet (dry) years since the resultant soil wetness enters into the sensitive range from a relatively insensitive range [25].

In China and its surrounding regions, previous studies have paid more attention to the spatial distribution and seasonal changes of L–A coupling, based on monthly, 10-day, pentad, or daily data and pointed out that there are obvious differences in the coupling strengths calculated from data at different time scales [26–28], but with a lack of research on daytime-only L–A coupling characteristics. Since the processes through which solar radiation affects the distribution of energy at the surface are mainly concentrated during the daytime, the land–atmosphere coupling metrics should focus on the processes affected by the heating of solar radiation during the daytime and the research with daytime-only mean data is conducive for enhancing the understanding of L–A coupling [29,30]. In addition, both large interannual and intraseasonal variations in soil moisture during the warm season in China and its surrounding areas exist, especially northern China [31]. Because of the existence of an insensitive range of soil moisture in evapotranspiration regimes and the high sensitivity of soil moisture–atmosphere coupling to climate change [32], L–A coupling

may show fluctuations with the change in soil wetness. The simple averaging of the L–A coupling strengths for all soil moisture conditions leads to coupling signal loss. Therefore, it is necessary to explore the coupling strength under different soil moisture backgrounds, which is helpful for predicting extreme weather events or climate change.

Overall, this research comprises two major parts. First, we investigate the strength of the L–A coupling under different soil moisture conditions during the warm season in China and its surrounding regions. Furthermore, we utilize the Weather Research and Forecasting (WRF) model to carry out the sensitivity experiments to investigate the impact of soil moisture anomalies on L–A coupling in the North China Plain, which is one of the hotspots in L–A coupling and is prone to droughts and preliminarily discussion of the effects of SM anomalies on the risk of drought.

2. Data and Methods

2.1. Study Region

This paper focuses on China and its surrounding areas (mainly India) as the study area. The East Asian region, where China is situated, is bordered by the Pacific Ocean to the east, the Indian Ocean to the south, and the Tibetan Plateau to the west. Figure 1 depicts a map of elevation, which generally shows a gradual decrease from west to east. The area has various surface features and is influenced by the monsoons during warm seasons, exhibiting varying climatic conditions [33].
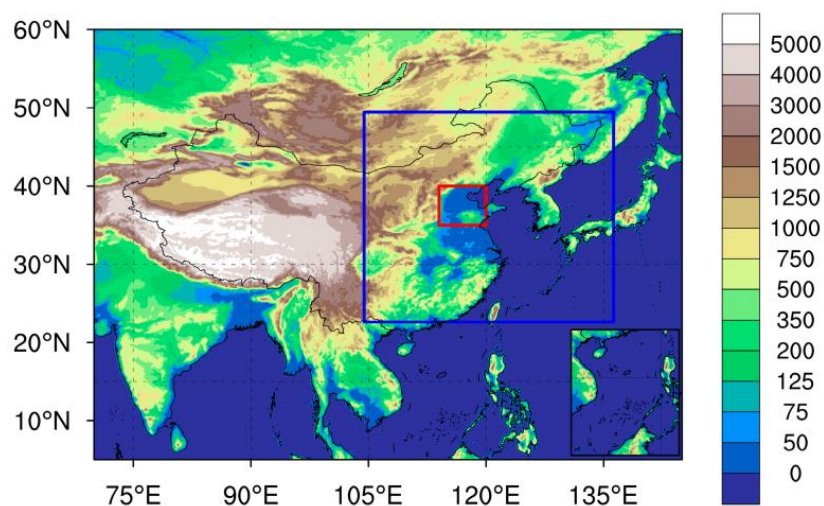

Figure 1. Topography (units: m) in China and its surrounding areas. The elevation data are from the Global 30 Arc-Second Elevation (GTOPO30 10 min) dataset: https://lta.cr.usgs.gov/GTOPO30 (accessed on 22 January 2024). The blue box represents the model simulation domain. The inner red box represents the area where soil moisture is modified in four sensitivity experiments.

2.2. ERA5 Data

The study of L–A coupling has been constrained due to the lack of observational data for a long period [34,35]. The development of reanalysis datasets provides time-continuous and global data for research, which can compensate for the lack of ground-based observations and satellite data [27]. In this study, we have employed ERA5 (the fifth-generation reanalysis dataset from the European Centre for Medium-Range Weather Forecasts) [36]. The ERA5 reanalysis data have been proven to be highly applicable at daily, monthly, and annual scales, offering higher spatial and temporal resolution and more accurate global precipitation and evapotranspiration compared to ERA-Interim [36]. ERA5 data accurately capture the daily cycle of summer precipitation in the North China Plain [37]. Sun et al. [38] compared the precipitation, surface latent and sensible heat (SH) fluxes, boundary layer height, 2 m temperature, and specific humidity in the Tibetan Plateau of ERA5 with observational data, indicating that the variables in ERA5 are relatively

reliable. A large number of studies have used ERA5 for the research of L–A coupling in China or globally. Yin et al. [30] calculated the strength of global L–A coupling using ERA5 data at different time scales and the "hot spots" were consistent with the GLACE experiment [16,39]

In this study, hourly ERA5 reanalysis data at $0.25° \times 0.25°$ horizontal sampling are used for statistical analysis, including 0–7 cm soil moisture (SM [m^3/m^3]), latent heat flux (LH [W/m^2]), 2 m temperature (T_{2m} [K]), dew point temperature (D_{2m} [K]), horizontal winds (U-component of wind, V-component of wind [m/s]), and specific humidity (q [kg/kg]). The study period is the warm season (from May to September) from 1981 through 2020.

2.3. Methods

2.3.1. Land–Atmosphere Coupling Strength

The land–atmosphere coupling strength represents the extent to which the atmosphere responds to anomalies in the state of the land surface [39]. The estimates of L–A feedback typically use linear statistical methods (e.g., correlation coefficients and linear regression) or numerical simulation experiments [2,39–41], among which the two-legged index can better represent the coupling strength than correlation alone [40,41]. It divides the coupling in the L–A interaction chain into two steps: a land leg and an atmospheric leg. The land section represents the coupling between the state of the land (typically soil moisture) and surface heat, moisture, or momentum flux. The atmospheric leg is the coupling between the land surface flux and the atmospheric state.

The metrics can be formulated as follows [40,41]:

$$I_{SM-LH} = \frac{dLH}{dSM}\sigma_{SM} = \rho(SM, LH) \times \sigma_{LH} \tag{1}$$

$$I_{LH-LCL} = \frac{dLCL}{dLH}\sigma_{LH} = \rho(LH, LCL) \times \sigma_{LCL} \tag{2}$$

where I_{SM-LH} and I_{LH-LCL} are the coupling strengths of the land and atmospheric leg, respectively; ρ represents the correlation coefficient between two variables; σ is the standard deviation; and SM, LH, and LCL (lifting condensation level) represent the land state, the surface flux, and the atmosphere, respectively. The LCL (m) can be estimated from T_{2m} and D_{2m}: $LCL = 125 \times (T_{2m} - D_{2m})$.

We calculated the L–A coupling strength based on daytime-only mean data. The daytime-only mean data were obtained by averaging the time steps between 08:00 and 20:00 local time [30]. Before calculating the coupling strength, the daytime-only mean data were first de-trended and de-seasonalized cyclically to reduce the effects of seasonal differences [27]. Based on the above method, a coupling index was obtained for each month during the warm season of each year at each grid point. We calculated the coupling indexes in the region (5° N–60° N, 70° E–140° E), encompassing the whole of China and India. To study the differences of the coupling under different climatic conditions, the 200 months (warm seasons of 40 years) were classified into the following three types according to the monthly soil moisture anomalies for each grid point: wet (60 months in total, with 12 wet samples in each of the months of May–September; the criterion for the selection of the wet month for a given grid point is that the average SM for that month must be greater than the 70th percentile), neutral (80 months, with 16 intermediate months in each of May–September; an intermediate sample was selected if the average SM in that month lies between the 30th and 70th percentiles), and dry (60 months, with 12 dry soil months in each of May–September; a dry month was selected when the average SM in that month is less than the 30th percentile). The samples for each grid point varied between dry, neutral, and wet months. The land and atmosphere leg metrics were calculated for the three SM scenarios.

2.3.2. Model Setup

In order to further investigate the mechanism of L–A interactions under different soil moisture conditions and the potential influence on regional precipitation, we employed WRF 4.0 for sensitivity experiments. Four sets of soil moisture sensitivity experiments were conducted: driest, dry, wet, and wettest. We decoupled the evolution of SM with the atmosphere by replacing the initial value of SM with a constant value. With the above approach, the SM influenced atmospheric variables but the changes in these variables were not fed back to the SM, providing a more intuitive reflection of how atmospheric status changed with soil wetness. The initial soil conditions for the first layer were from ERA5. The maximum SM value in this dataset within the study area during the warm seasons of 2011–2020 was about 0.447 m^3/m^3 and the minimum was near 0.07 m^3/m^3. The soil moisture in the North China Plain (35–40° N, 114–120° E; Figure 1) in the four sets of sensitivity experiments changed to 0.07, 0.196, 0.322, and 0.447, respectively.

In this study, we conducted four soil wetness initializations for 10 warm seasons, totaling 40 WRF simulations (4 SM levels × 10 years). The meteorological initial and lateral boundary conditions were derived from ERA5 reanalysis data updated every 6 h with a spatial resolution of 0.25° × 0.25°. The simulation domain was centered at (116.8° E 34.2° N), with horizontal grid points 91 × 102 (the grid distance is 30 km) and 38 nonuniform layers in the vertical resolution. The simulation area is shown in Figure 1. Each simulation ran from May 1 to September 30 of 2011–2020 with output every 3 h. The first 15 days were considered as the model spin-up period, so the data from May 15 to September 30 were utilized in the analysis. The schemes adopted in this study include the YSU boundary layer scheme, the WSM6 microphysics scheme, the Kain–Fritsch convective parameterization scheme, the rapid radiation transfer model (RRTM) long-wave radiation scheme, the Dudhia short-wave radiation scheme, the Monin–Obukhov surface layer scheme, and the Noah land surface scheme. The combination of parameterization schemes has been shown to perform well in the forecast skill [42]. Therefore, the results of the tests conducted using the aforementioned model setup can serve as the foundation for the analysis in this paper.

2.3.3. Vertically-Integrated Moisture Flux Convergence (VIMFC)

The water vapor transport due to the effects of synoptic forcing is an important component of the atmospheric moisture balance in the domain and is the main source for summer precipitation over most land areas. When the region is influenced by large-scale atmospheric processes (more external moisture supply), will it inhibit the process of energy or heat exchange between the land and the atmosphere? To address this question, we used VIMFC to characterize the water vapor transport in the domain, which is calculated as follows [43]:

$$VIMFC = -\nabla \cdot \frac{1}{g} \int_0^{P_s} (\mathbf{V}q)dp \tag{3}$$

where g is the gravitational acceleration, P_s is the surface pressure, $\mathbf{V}$ represents the horizontal wind vector, and q is specific humidity. A positive VIMFC value indicates the convergence of water vapor, which is beneficial for regional precipitation. The monthly mean VIMFC values for 2011–2020 warm seasons (50 months) are calculated by ERA5 data.

3. Results

3.1. Regional Characteristics and Intraseasonal Evolution of Daytime Land–Atmosphere Coupling under Different SM Conditions

We first analyze the characteristics of L–A coupling under different SM conditions in China and its surrounding areas. From the spatial distribution (Figure 2a–c), it can be seen that both the coupling metrics of land and atmosphere segments differ in dry and wet soil months. The positive land leg metrics indicate that evapotranspiration is mainly limited by SM and, conversely, controlled by energy. So, we mainly focus on the positive SM–LH coupling region. In north-northeast China, the Yunnan-Guizhou Plateau, and part

of the Southeast Coast, the SM–LH feedback is positive under dry soil conditions, while the above areas are negatively coupled under wet conditions. In the mid-latitude arid zone of China and the Great Indian Desert region, the positive coupling strength under wet months is significantly stronger than that under dry soil, indicating that evapotranspiration in this region is greatly limited by SM and the LH decreases significantly with decreasing SM.
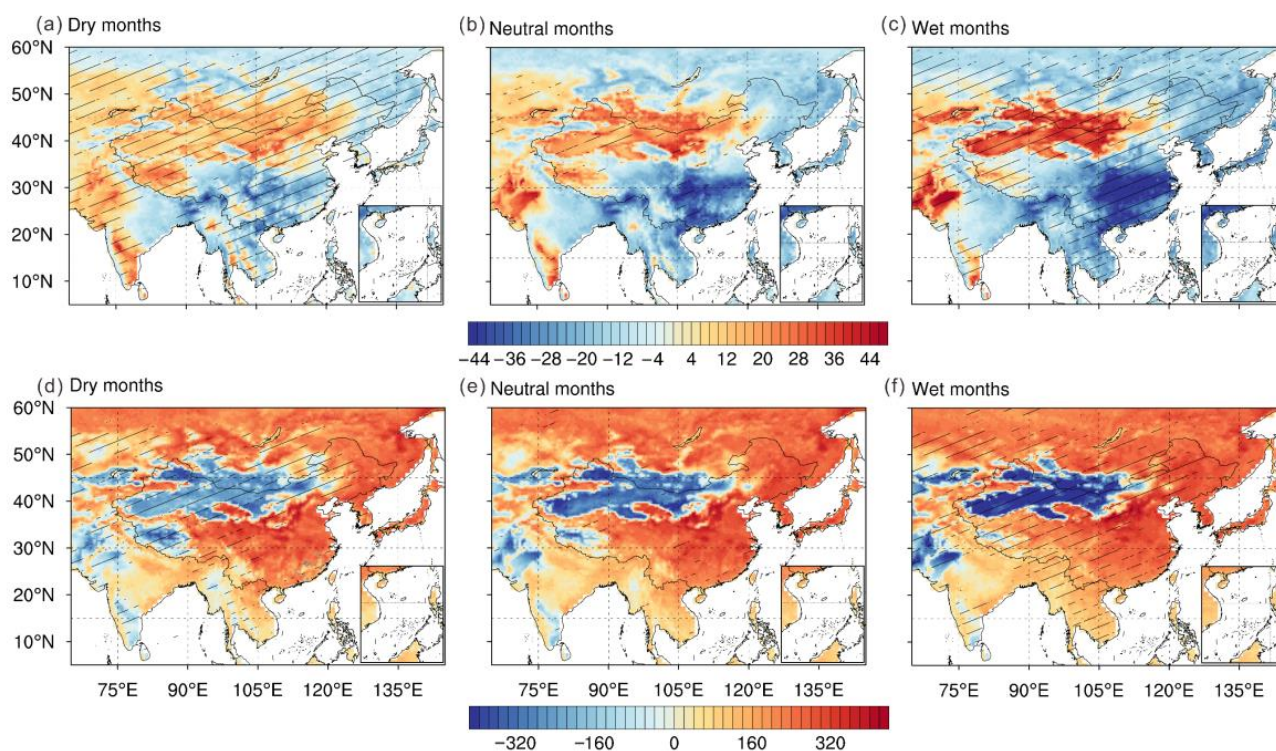

Figure 2. Spatial distribution of SM–LH ((**a**–**c**); W/m^2) and LH–LCL ((**d**–**f**); m) coupling indices for dry, neutral, and wet soil months. The region with the slash is the area that passes the 95% significance test, indicating that there is a significant difference between the samples' coupling strength and the whole.

From the evolution of the fitted curves with the spatial percentile of climatological mean SM (Figure 3), it can be seen that in the drier regions (with smaller values of the horizontal coordinates below 0.2), there is a positive SM–LH coupling in the three climatic scenarios and the coupling strength is strongest in wet conditions (e.g., arid areas of northwest China and the Great Indian Desert region in Figure 2). When the value of the cross-axis coordinates is about 0.2, there is an intersection of the dry and wet fitted lines and to the right of the intersection, the dry months fitting line is located above the wet, indicating that if the SM spatial percentile at a given point is greater than 0.2, the positive coupling between SM and LH is stronger for dry soil conditions than for wet. Moreover, in the area whose spatial percentile of mean SM between 0.3 and 0.5, from dry to wet soil months, the fitted land segment index changes from positive to negative (e.g., north-northeast China in Figure 2). Eventually, all of the three fitted curves decrease to negative values and the strongest negative coupling occurs under wet conditions. This may be attributed to the higher likelihood of precipitation in wetter climatic conditions, resulting in the suppression of evaporation. Preliminary results show that the distribution of SM–LH coupling strength exhibits clear regional characteristics under different SM conditions.
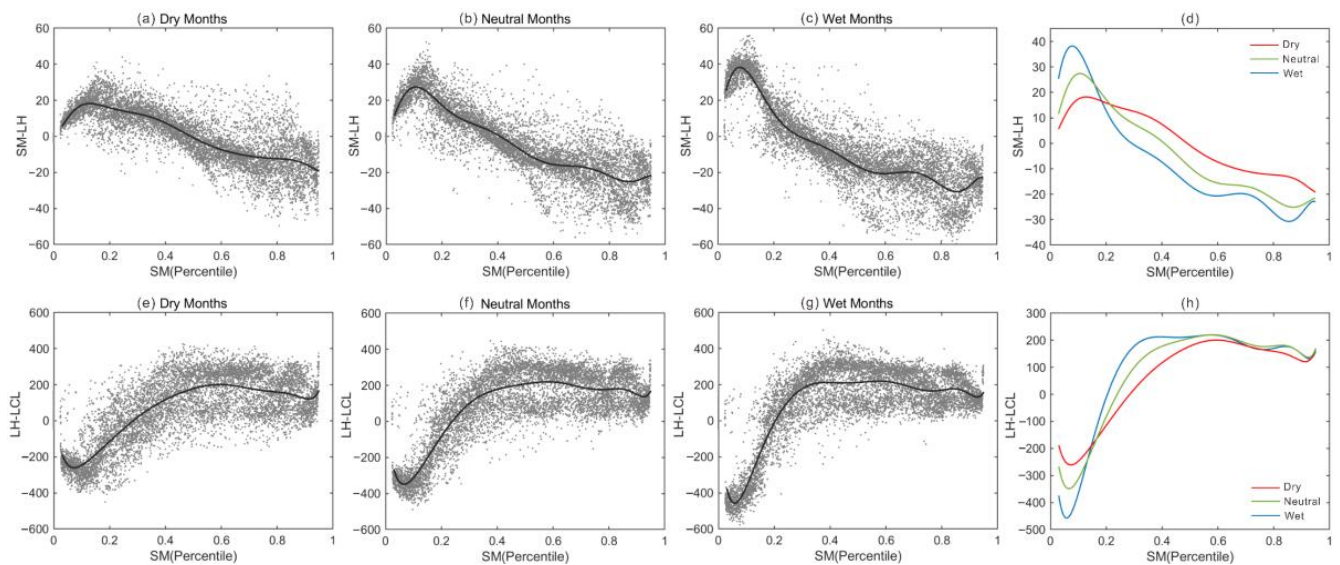
Figure 3. Scatterplots and fitted curves of the coupling strength of SM–LH ((**a**–**d**); W/m^2) and LH–LCL ((**e**–**h**); m) for dry, neutral, and wet months as a function of the spatial percentile of warm-season soil wetness climatology. The curves are obtained from a 10-degree polynomial curve fitting.

According to the local land–atmosphere coupling chain [44], the evapotranspiration can further influence water vapor within the boundary layer. The more abundant water vapor is often accompanied by lower LCL, which is conducive to precipitation. As a result, for the coupling between LH and LCL (atmospheric leg), we focus on regions where the coupling index is negative. The spatial patterns of LH–LCL coupling strength (Figure 2d–f) show that in northwest China, Hetao, the Tibetan Plateau, and the Great Indian Desert regions, the coupling strengths of the atmospheric segments synthesized from both the dry and wet month samples are significantly different from all warm season months. Specifically, in the mid-latitude arid area and the Great Indian Desert, the LH–LCL coupling is stronger under wet months, whereas on the Tibetan Plateau, in contrast, it is stronger under dry. In Yunnan and parts of Southeast Asia, it also shows weak negative LH–LCL coupling under dry conditions. Likewise, the evolution of the fitted curves (Figure 3e–h) reveals significant differences in the distribution of LH–LCL coupling under different soil wetness months in dry and intermediate range soil moisture.

To further investigate regional characteristics of the two-legged metrics under different soil moisture conditions, based on the multi-year average distributions of regional percentiles of warm-season mean soil wetness and standard deviation of SM (Figure 4), the entire research area is divided into the following nine subregions [33]: northeast China (I, 43–54° N, 110–135° E), northern China (II, 35–43° N, 110–124° E), Jianghuai (III, 29–35° N, 110–123° E), Southeast China (IV, 18–29° N, 110–123° E), Hetao (V, 35–43° N, 96–110° E), Southwest China (VI, 21–35° N, 96–110° E), northwest China (VII, 35–49° N, 73–96° E), the Tibetan Plateau (VIII, 27–35° N, 78–96° E), and India (IX, 14–27° N, 70–85° E). The relationship between the coupling strength and SM anomalies for different warm-season months in each subregion and the intraseasonal variation are summarized in Figure 5. In northeast and northern China, with the shift of SM from negative to positive anomalies, there is also a shift of SM−LH coupling from positive to negative, especially in May and June. In Jianghuai, southeast, and southwest regions, the land surface segment coupling index is negative in most months of the warm season and it is considered that no significant L–A feedback occurs in all months in this region. However, the intraseasonal variation in the coupling in southeast China is very obvious and the negative coupling is significantly stronger in May and June than in other months because of much precipitation during the first rainy season precipitation in South China and the abundant water vapor inhibits evaporation. In the mid-latitude arid regions (Hetao and northwest China), the index of land surface segment

is positive in all months and in the northwest, there is a clear tendency for the positive coupling strength to increase as the regional average soil becomes wetter. The coupling strength is weakest in September in the two regions and the difference in SM–LH coupling between other months is not significant. There is also an intraseasonal change in the index sign in Tibet and India, with a positive SM–LH coupling in May and June and a negative from July to September.
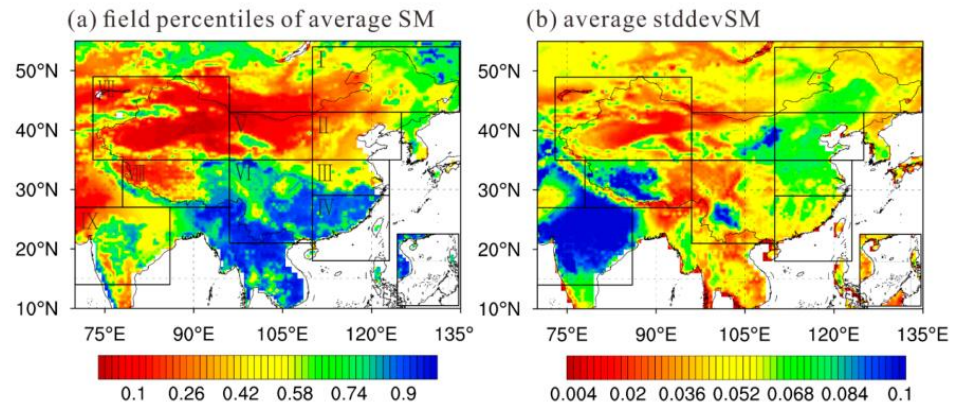

Figure 4. Distribution of spatial percentiles of the warm-season climatological mean soil wetness (**a**) and average standard deviation of SM over 40 warm seasons ((**b**), m^3/m^3).
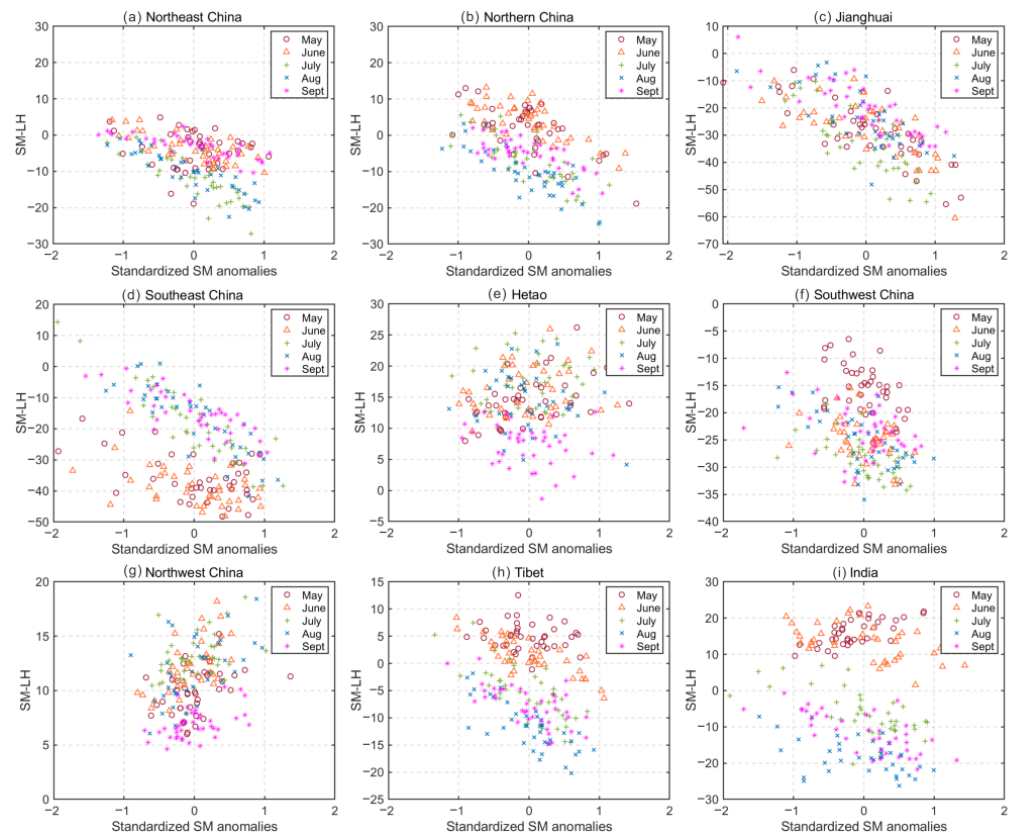

Figure 5. Relationships between the regionally averaged standardized SM anomalies and SM–LH coupling index for each month of the 40-year warm season in nine subregions.

Intraseasonal variations in the strength of LH–LCL coupling in different regions and the variation in the atmospheric segment coupling with SM anomalies for each month are shown in Figure 6. A negative regional average LH–LCL coupling index exists in

the Hetao, northwest China, Tibet, and India. In Hetao and northwest China, a negative coupling becomes strong in May but the intraseasonal variation trend is not obvious in other months. In the Tibetan Plateau, there is a clear difference in the coupling strength between months with stronger negative coupling in May–June, followed by July, and with the shift from negative to positive SM anomalies, the regional average index shifts from negative to positive values in May–July and the positive coupling is observed in August–September, regardless of the SM conditions. Unlike Tibet, the variation in atmospheric segment coupling with SM anomalies in India is not obvious in all five months and also shows significant intraseasonal variations, with the LH–LCL index being mostly negative in May and June, gradually shifting to a positive coupling in July, with the positive coupling being the strongest in August–September.
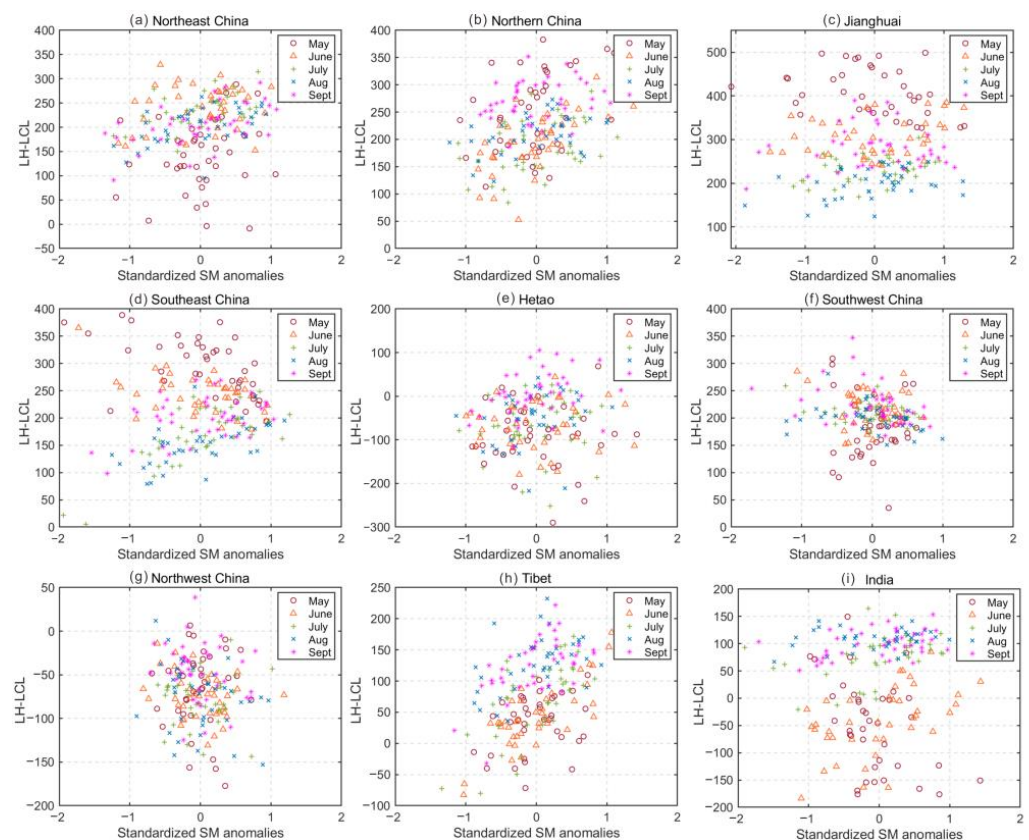

Figure 6. Relationships between the regionally averaged standardized SM anomalies and LH–LCL coupling index for each month of the 40-year warm season in nine subregions.

From the above analysis, it can be concluded that the distribution of the daytime-only coupling strength under different SM conditions has obvious regional characteristics: in the arid (humid) region, the SM–LH coupling strength is enhanced as the SM becomes wetter (dryer) and in the semi-arid/semi-humid region, as the soil becomes wetter, the land surface segment coupling index shifts from positive to negative. The impact of SM anomalies on daytime-only atmospheric segment coupling is weaker than on land segments and the shift in coupling signals only exists in Tibet. Due to the influence of the summer monsoon, there is an intraseasonal signal conversion of SM–LH feedback (from positive coupling to negative) in North China, the Tibetan Plateau, and India, whereas in the atmospheric segment, the signal conversion only occurs in India.

3.2. Sensitivity Experiments of Impact of SM Anomalies on L–A Coupling in the North China Plain

The evaporative fraction [EF = LH/(LH + SH)] in soil moisture-limited regions is dependent on soil moisture and the feedback between soil moisture and evapotranspiration is the basis for the soil moisture–precipitation feedback. In regions dominated by the energy-limited regime, the EF is independent of SM. From the statistical analysis, it can be seen that both the land and atmospheric segments in North China are sensitive to SM. In order to explain the influence of different soil moisture conditions, we conducted soil moisture sensitivity experiments in North China and the model setup is shown in Section 2.3.2.

The results of LH (Figure 7) and SH (Figure 8) under different soil moisture experiments show that in May and June, the LH gradually increases from the driest to wettest test regardless of the advected atmospheric moisture, while the SH is opposite, suggesting that the distribution of surface fluxes is strongly influenced by SM and that the daytime-mean EF also has evident differences in various experiments (Figure 9a,b) in May and June. At this time, evapotranspiration is characterized by the soil moisture-limited regime. Furthermore, with more moisture inflow, LH is higher in drier soil experiments (driest and dry) and the SH is lower, while in wetter experiments (wettest and wet), there is little difference in heat flux between different years. From July onwards, North China is influenced by the East Asian summer monsoon and the effect of soil wetness on the distribution of heat flux is not as pronounced as in the pre-monsoon period (May and June) under any state of incoming moisture but the EF still increases significantly from the driest to the wettest experiments. Changes in LH and SH under the wet-to-wettest tests are minimal, so the differences in daytime-mean EF (Figure 9d,e) between the two wetter experiments are small. The above analysis indicates that from July to September, the evapotranspiration mechanism in the North China Plain is dominated by a soil moisture-limited regime in the drier SM state and becomes energy-limited in the wet soil state, with corresponding regional average soil moisture values ranging from 0.24 to 0.29 m^3/m^3.

The maximum sensible and latent heat flux both occur in the late afternoon (Figure 10). The larger SH in the drier experiments produces more turbulent kinetic energy, which is favorable to the rising of the planetary boundary layer height (PBL) and the smaller LH is unfavorable for the lowering of the LCL. As a result, the PBL and the LCL increase from the wettest to the driest experiments in each month. In May–June, the LCL and PBL in four soil moisture tests differ significantly, which is due to the fact that the heat flux during the pre-monsoon period is greatly affected by SM, resulting in significant differences in flux distribution across different experiments. In August and September, the EF in the two wetter tests changed a little, resulting in the PBL and LCL of the two experiments being relatively close, which confirms that at wet soil levels, the North China Plain is an energy-limited evaporative regime and the alteration of surface flux caused by soil moisture has little effect on the atmosphere.

A height of PBL above the LCL is a necessary but insufficient condition for triggering convective precipitation [24]. A day is defined as a "crossover event" if the top of PBL reaches the LCL at any time during the day (from 05:00 the first day to 05:00 the following day). Figure 11 shows the probability of crossover events in the four SM experiments from May to September. The strength of the coupling can be reflected by the extent to which the probability of the crossover events varies with SM. If soil moisture fluctuates, the likelihood of convective triggering also varies significantly, which indicates that soil moisture has a significant impact on the state of the atmosphere (strong coupling). During the pre-monsoon period (May and June), the probability of crossover events increases as the soil becomes wetter, indicating that it is more favorable for convection triggering when the soil gradually becomes wet. From the driest to the wet tests in July–September, the crossover events show the same change pattern with soil moisture, while from the wet to the wettest experiments, the probability does not change much. These results confirm that

a strong positive L–A feedback exists during the warm season in North China Plain when the soil becomes dry enough.
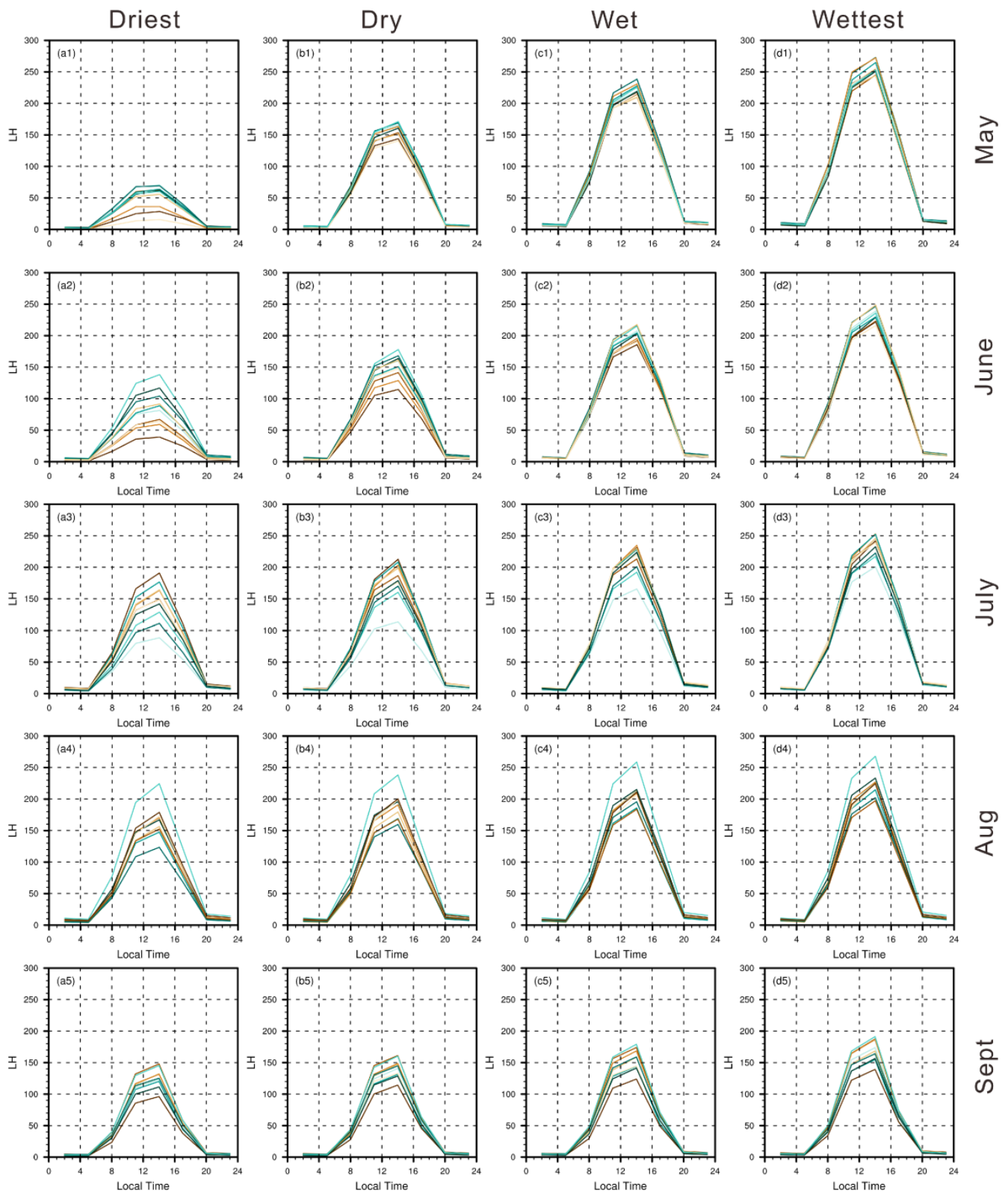

Figure 7. Area-averaged LH in May–September of different years at four soil moisture levels (**a1**–**d5**). The rows represent the months from May to September. The columns represent four sets of experiments. A line with a greener color indicates higher moisture inflow in that month.
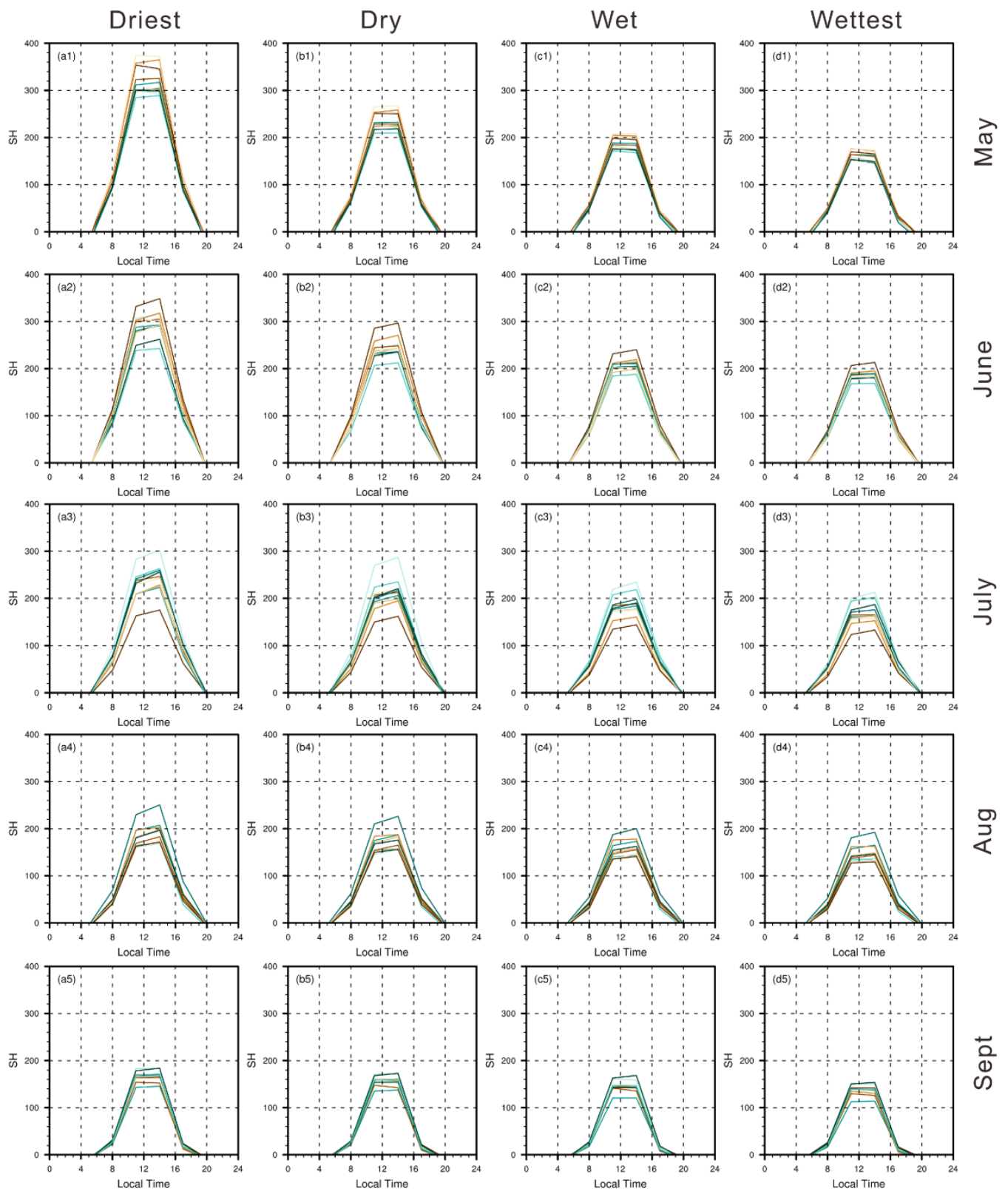
Figure 8. Area-averaged SH in May–September of different years at four soil moisture levels (**a1–d5**). The rows represent the months from May to September. The columns represent four sets of experiments. A line with a greener color indicates higher moisture inflow in that month.
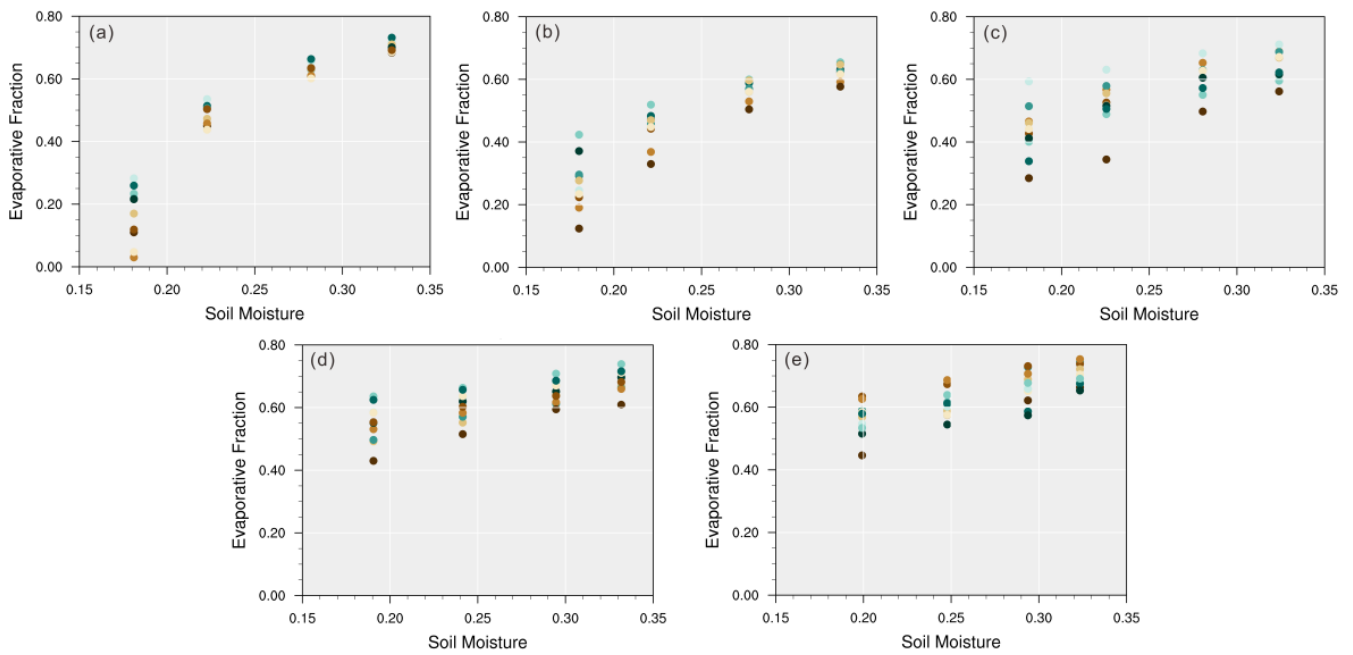
Figure 9. Area- and daytime-averaged EF in May (**a**), June (**b**), July (**c**), August (**d**) and September (**e**) of different years at four SM levels. A greener colored dot represents the month with higher moisture inflow. The four soil moisture values on the horizontal axis for each month represent the average of the model output data from four sets of experiments conducted during that month.
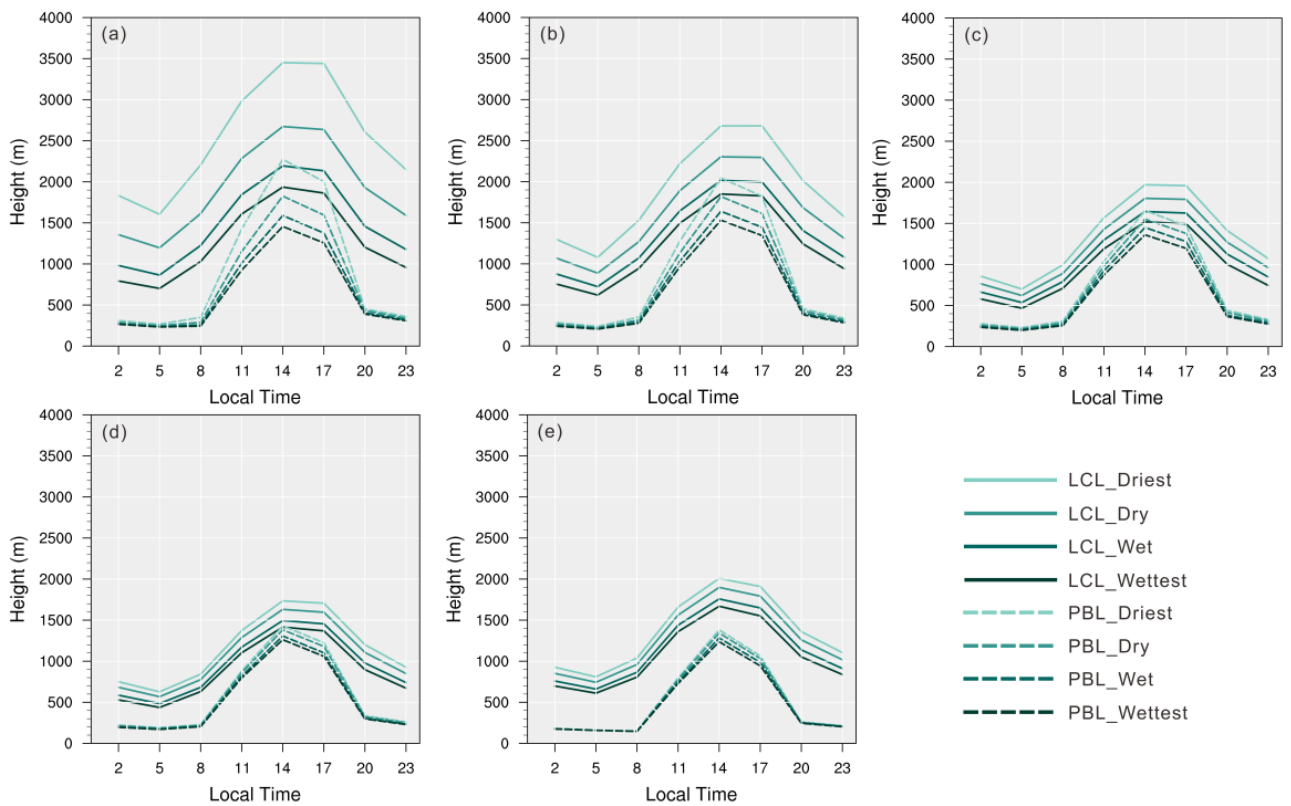

Figure 10. The evolution of area-averaged LCL (solid lines) and PBL (dashed lines) in May (**a**), June (**b**), July (**c**), August (**d**) and September (**e**) under different soil moisture sensitivity experiments.
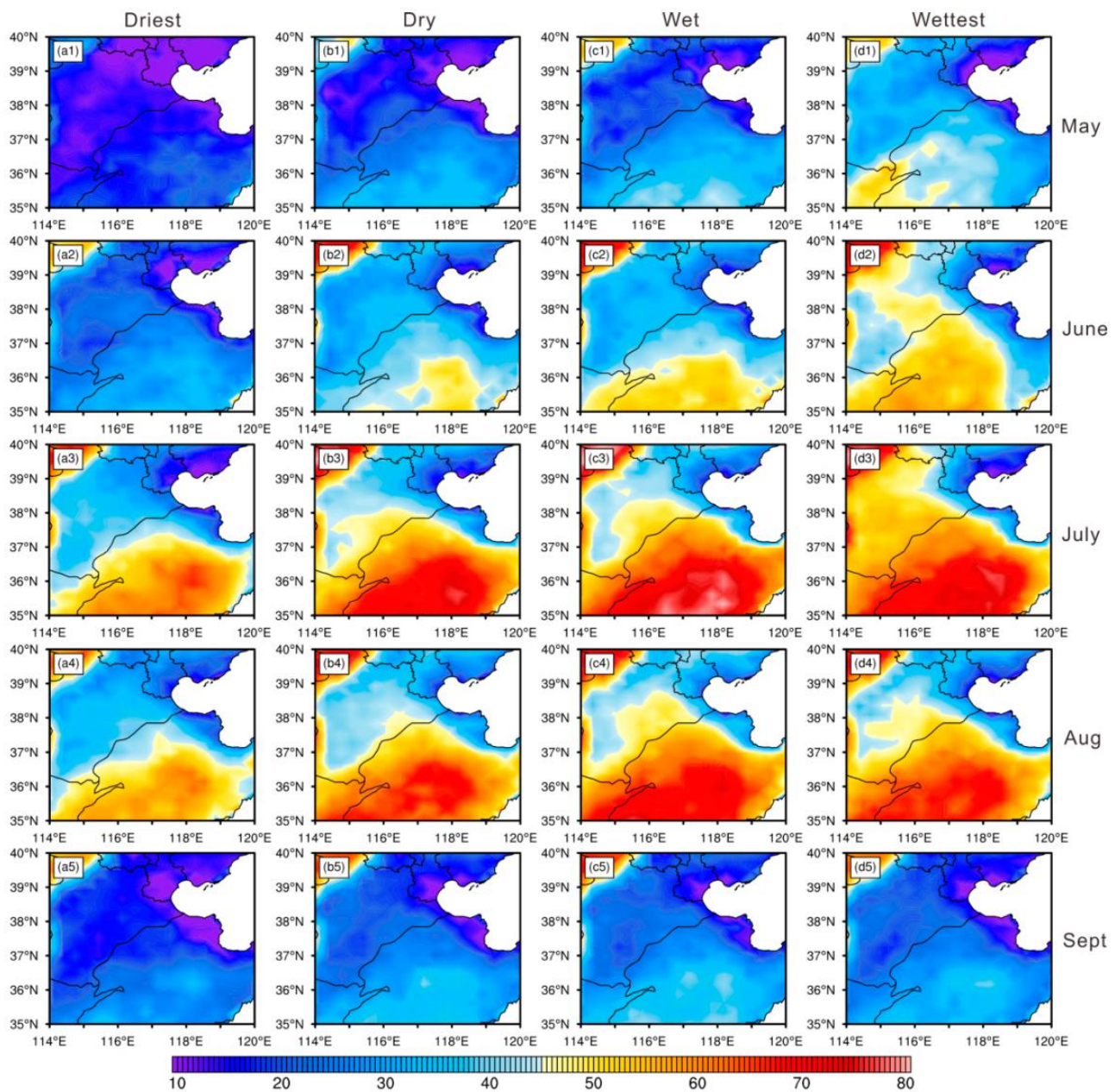
Figure 11. Probability of crossover events between LCL and PBL in four experiments for each warm-season month (**a1–d5**). The rows represent the months from May to September. The columns represent four sets of experiments.

4. Discussion

Previous studies on critical zones for L–A coupling have combined coupling strengths across all climatic contexts [27,35], which may result in weakened or lost coupling signals. The interaction between soil moisture and evapotranspiration forms the basis of the soil moisture–precipitation feedback. The impact of soil moisture on evapotranspiration does not increase linearly; instead, there are sensitive intervals. It is necessary to separate the statistics of the coupling strength at different soil moisture levels. This article indicates that the coupling strength varies significantly with soil moisture conditions (see Figure 2). Strong coupling periods also occur in the areas found by the previous studies with weak coupling, such as the southeast coast and parts of the southwest of China. In these regions, the positive feedbacks generally occur when the soil becomes dry. North China is an arid/semi-arid region. Previous studies have indicated that this region exhibits strong

positive L–A coupling in summer [35]. However, this paper suggests that L–A coupling strength in North China is not strong when the soil becomes wetter and even that negative feedback exists.

Since the land segment index (SM–LH) varies with SM in North China (especially in the North China Plain), we isolate the effect of soil moisture on the atmosphere through sensitivity tests. In the North China Plain, the evaporative fraction and atmosphere conditions (probability of occurrence of crossover events) in relatively dry soil states respond dramatically to changes in soil moisture (Figure 11), implying the strong positive L–A coupling. Furthermore, the external moisture supply does not reverse the characteristics of the change in evaporation fraction with soil moisture (Figure 9) and the soil moisture-limited evapotranspiration mechanism still develops even if there is sufficient moisture inflow. Positive L–A coupling reduces the system's ability to regulate moisture in strong land–atmosphere coupling zones [45]. In the circumstances with negative SM anomalies, less evapotranspiration leads to unfavorable atmospheric conditions for precipitation and the high surface sensible heat flux may increase the surface temperature, which may aggravate soil drought and extreme hot temperatures [45–47]. Once a drought occurs, strengthened positive land–atmosphere coupling resulting in reduced precipitation will further exacerbate the drought [48]. In the case of negative feedback, the L–A system can better regulate the moisture content and convective precipitation is more likely to be triggered when the soil is dry [23,49]. Soil drought and atmosphere aridity depend on the local L–A coupling and are expected to intensify in the 21st century [50,51]. The L–A coupling in regions such as the northeastern United States will be considerably strengthened due to soil moisture-limited evapotranspiration mechanisms under dry soil moisture conditions [48]. Similarly, in the North China Plain, if the soil moisture experiences a negative anomaly during the initial phase of the warm season, which in turn leads to a decrease in precipitation due to positive feedback, it foreshadows an increased risk of drought.

5. Conclusions

In this study, the distribution of daytime-only mean L–A coupling under different soil moisture conditions is analyzed synthetically and it is found that the distribution of the coupling strengths in the warm season under different soil moisture conditions has obvious regional characteristics. The whole study area (China and its surrounding areas) is divided into nine subregions to analyze the variation in the coupling strength with soil moisture anomalies in each month within the warm season. As soil wetness becomes wetter, the positive coupling of the land leg (SM–LH) is enhanced in arid regions (e.g., the northwest China and Hetao) and in semi-arid/half-humid regions (e.g., the northeast and northern China) the coupling signal shifts from positive to negative. Due to the influence of the summer monsoon, there is an intraseasonal signal conversion of SM–LH feedback in North China, the Tibetan Plateau, and India, from positive to negative coupling before and after the monsoons. For the atmospheric leg between LH and LCL, the differences between months are not significant in North China but the LH–LCL coupling varies with soil moisture anomalies.

The WRF model is utilized to conduct four sets of sensitivity experiments with different soil moisture levels across 10 years in North China Plain, further exploring the mechanism of evapotranspiration and the impact of large-scale atmospheric processes (external moisture advection) on the coupling under different soil moisture conditions. The results show that regardless of external moisture inflow, the surface sensible and latent heat fluxes in the North China Plain in May and June are largely determined by soil moisture, so the evapotranspiration is considered to be soil moisture-limited at this time. From July to September, a soil moisture-limited evapotranspiration regime still occurs under relatively dry soil conditions, while the energy-limited regime occurs when soil becomes wet, with the critical area-averaged soil moisture value separating a soil moisture-limited and an energy-limited regime lying between 0.24 m^3/m^3 and 0.29 m^3/m^3.

It is worth noting that this study is subject to certain uncertainty. Due to the limited availability of high spatial and temporal resolution, we relied solely on the reanalysis dataset (ERA5) for our statistical analysis. In the sensitivity tests, we only utilized the results from one combination of parameterization schemes. Further validation is necessary to determine if similar results can be drawn from other sources. Multiple studies have been conducted to construct drought indexes based on local L–A coupling or evapotranspiration characteristics [52–54]. We only point out that the positive feedback under dry soil conditions might increase the risk of drought through discussion and the mechanism of L–A coupling on drought should be further explored in depth.

Author Contributions: Conceptualization, L.W., S.Z. and X.Y.; methodology, L.W.; software, L.W.; validation, L.W., X.Y. and C.H.; formal analysis, L.W.; investigation, L.W.; resources, S.Z.; data curation, L.W.; writing—original draft preparation, L.W.; writing—review and editing, L.W. and S.Z.; visualization, L.W.; supervision, S.Z.; project administration, S.Z.; funding acquisition, S.Z. All authors have read and agreed to the published version of the manuscript.

Institutional Review Board Statement: Not applicable.

Informed Consent Statement: Not applicable.

Data Availability Statement: The ERA5 hourly reanalysis data are publicly available at https://doi.org/10.24381/cds.adbb2d47 and were accessed in September 2022.

Conflicts of Interest: The authors declare no conflict of interest.

References

1. Santanello, J.A.; Dirmeyer, P.A.; Ferguson, C.R.; Findell, K.L.; Tawfik, A.B.; Berg, A.; Ek, M.; Gentine, P.; Guillod, B.P.; Van Heerwaarden, C.; et al. Land-Atmosphere Interactions the LoCo Perspective. *Bull. Am. Meteorol. Soc.* **2018**, *99*, 1253–1272. [CrossRef]
2. Seneviratne, S.I.; Lüthi, D.; Litschi, M.; Schär, C. Land-Atmosphere Coupling and Climate Change in Europe. *Nature* **2006**, *443*, 205–209. [CrossRef]
3. Seneviratne, S.I.; Corti, T.; Davin, E.L.; Hirschi, M.; Jaeger, E.B.; Lehner, I.; Orlowsky, B.; Teuling, A.J. Investigating Soil Moisture-Climate Interactions in a Changing Climate: A Review. *Earth-Science Rev.* **2010**, *99*, 125–161. [CrossRef]
4. Hu, H.; Leung, L.R.; Feng, Z. Early Warm-Season Mesoscale Convective Systems Dominate Soil Moisture–Precipitation Feedback for Summer Rainfall in Central United States. *Proc. Natl. Acad. Sci. USA* **2021**, *118*, e2105260118. [CrossRef] [PubMed]
5. Zhang, S.; Yang, X.; Zhang, W.; Li, S.; Zhang, Y. Sensitivity of Afternoon Precipitation to Evaporative Fraction in Eastern Asia Based on ERA-Interim Datasets. *Atmos. Sci. Lett.* **2019**, *20*, 2–7. [CrossRef]
6. Zheng, Y.; Kumar, A.; Niyogi, D. Impacts of Land–Atmosphere Coupling on Regional Rainfall and Convection. *Clim. Dyn.* **2015**, *44*, 2383–2409. [CrossRef]
7. Koster, R.D.; Chang, Y.; Wang, H.; Schubert, S.D. Impacts of Local Soil Moisture Anomalies on the Atmospheric Circulation and on Remote Surface Meteorological Fields during Boreal Summer: A Comprehensive Analysis over North America. *J. Clim.* **2016**, *29*, 7345–7364. [CrossRef]
8. Berg, A.; Lintner, B.; Findell, K.; Giannini, A. Soil Moisture Influence on Seasonality and Large-Scale Circulation in Simulations of the West African Monsoon. *J. Clim.* **2017**, *30*, 2295–2317. [CrossRef]
9. Zuo, Z.; Zhang, R. Influence of Soil Moisture in Eastern China on the East Asian Summer Monsoon. *Adv. Atmos. Sci.* **2016**, *33*, 151–163. [CrossRef]
10. Miralles, D.G.; Gentine, P.; Seneviratne, S.I.; Teuling, A.J. Land–Atmospheric Feedbacks during Droughts and Heatwaves: State of the Science and Current Challenges. *Ann. N. Y. Acad. Sci.* **2019**, *1436*, 19–35. [CrossRef]
11. Dirmeyer, P.A.; Balsamo, G.; Blyth, E.M.; Morrison, R.; Cooper, H.M. Land-Atmosphere Interactions Exacerbated the Drought and Heatwave Over Northern Europe During Summer 2018. *AGU Adv.* **2021**, *2*, e2020AV000283. [CrossRef]
12. Dai, A. Increasing Drought under Global Warming in Observations and Models. *Nat. Clim. Chang.* **2013**, *3*, 52–58. [CrossRef]
13. Zhang, J.Y.; Wu, L.Y. Land-Atmosphere Coupling Amplifies Hot Extremes over China. *Chin. Sci. Bull.* **2011**, *56*, 3328–3332. [CrossRef]
14. Saini, R.; Wang, G.; Pal, J.S. Role of Soil Moisture Feedback in the Development of Extreme Summer Drought and Flood in the United States. *J. Hydrometeorol.* **2016**, *17*, 2191–2207. [CrossRef]

15. Wu, S.; Wei, Z.; Li, X.; Ma, L. Land-atmosphere Coupling Effects of Soil Temperature and Moisture on Extreme Precipitation in the Arid Regions of Northwest China. *Front. Earth Sci.* **2023**, *10*, 1079131. [CrossRef]

16. Koster, R.D.; Dirmeyer, P.A.; Guo, Z.; Bonan, G.; Chan, E.; Cox, P.; Gordon, C.T.; Kanae, S.; Kowalczyk, E.; Lawrence, D.; et al. Regions of Strong Coupling between Soil Moisture and Precipitation. *Science* **2004**, *305*, 1138–1140. [CrossRef]

17. Findell, K.L.; Gentine, P.; Lintner, B.R.; Kerr, C. Probability of Afternoon Precipitation in Eastern United States and Mexico Enhanced by High Evaporation. *Nat. Geosci.* **2011**, *4*, 434–439. [CrossRef]

18. Findell, K.L.; Eltahir, E.A.B. An Analysis of the Soil Moisture-Rainfall Feedback, Based on Direct Observations from Illinois. *Water Resour. Res.* **1997**, *33*, 725–735. [CrossRef]

19. Wei, J.; Dirmeyer, P.A. Dissecting Soil Moisture-Precipitation Coupling. *Geophys. Res. Lett.* **2012**, *39*, L19711. [CrossRef]

20. Denissen, J.M.C.; Teuling, A.J.; Pitman, A.J.; Koirala, S.; Migliavacca, M.; Li, W.; Reichstein, M.; Winkler, A.J.; Zhan, C.; Orth, R. Widespread Shift from Ecosystem Energy to Water Limitation with Climate Change. *Nat. Clim. Chang.* **2022**, *12*, 677–684. [CrossRef]

21. Hsu, H.; Dirmeyer, P.A. Soil Moisture-Evaporation Coupling Shifts into New Gears under Increasing CO_2. *Nat. Commun.* **2023**, *14*, 1162. [CrossRef] [PubMed]

22. Findell, K.L.; Eltahir, E.A.B. Atmospheric Controls on Soil Moisture-Boundary Layer Interactions. Part I: Framework Development. *J. Hydrometeorol.* **2003**, *4*, 552–569. [CrossRef]

23. Taylor, C.M.; De Jeu, R.A.M.; Guichard, F.; Harris, P.P.; Dorigo, W.A. Afternoon Rain More Likely over Drier Soils. *Nature* **2012**, *489*, 423–426. [CrossRef] [PubMed]

24. Siqueira, M.; Katul, G.; Porporato, A. Soil Moisture Feedbacks on Convection Triggers: The Role of Soil-Plant Hydrodynamics. *J. Hydrometeorol.* **2009**, *10*, 96–112. [CrossRef]

25. Guo, Z.; Dirmeyer, P.A. Interannual Variability of Land-Atmosphere Coupling Strength. *J. Hydrometeorol.* **2013**, *14*, 1636–1646. [CrossRef]

26. Zeng, D.; Yuan, X. Multiscale Land-Atmosphere Coupling and Its Application in Assessing Subseasonal Forecasts over East Asia. *J. Hydrometeorol.* **2018**, *19*, 745–760. [CrossRef]

27. Yang, Y.; Lin, Z.; Luo, L.; Zhong, L.; Jiang, D. Variation of Surface Air Temperature Induced by Enhanced Land–Atmosphere Coupling During 1981–2020 in Xinjiang, Northwest China. *J. Geophys. Res. Atmos.* **2023**, *128*, e2022JD037983. [CrossRef]

28. Yang, Z.; Zhang, Q.; Zhang, Y.; Yue, P.; Zhang, L.; Zeng, J.; Qi, Y. Hydrothermal Factors Influence on Spatial-Temporal Variation of Evapotranspiration-Precipitation Coupling over Climate Transition Zone of North China. *Remote Sens.* **2022**, *14*, 1448. [CrossRef]

29. Seo, E.; Dirmeyer, P.A. Understanding the Diurnal Cycle of Land-Atmosphere Interactions from Flux Site Observations. *Hydrol. Earth Syst. Sci.* **2022**, *26*, 5411–5429. [CrossRef]

30. Yin, Z.; Findell, K.L.; Dirmeyer, P.; Shevliakova, E.; Malyshev, S.; Ghannam, K.; Raoult, N.; Tan, Z. Daytime-Only Mean Data Enhance Understanding of Land-Atmosphere Coupling. *Hydrol. Earth Syst. Sci.* **2023**, *27*, 861–872. [CrossRef]

31. Wang, A.; Ma, X. An Overview of Soil Moisture Drought Research in China: Progress and Perspective. *Atmos. Ocean. Sci. Lett.* **2023**, *16*, 100297. [CrossRef]

32. Qiao, L.; Zuo, Z.; Zhang, R.; Piao, S.; Xiao, D.; Zhang, K. Soil Moisture–Atmosphere Coupling Accelerates Global Warming. *Nat. Commun.* **2023**, *14*, 4908. [CrossRef] [PubMed]

33. Chen, Y.; Yuan, H. Evaluation of Nine Sub-Daily Soil Moisture Model Products over China Using High-Resolution in Situ Observations. *J. Hydrol.* **2020**, *588*, 125054. [CrossRef]

34. Chen, H.; Yu, B.; Zhou, B.; Zhang, W.; Zhang, J. Role of Local Atmospheric Forcing and Land-Atmosphere Interaction in Recent Land Surface Warming in the Midlatitudes over East Asia. *J. Clim.* **2020**, *33*, 2295–2309. [CrossRef]

35. Gao, C.; Chen, H.; Sun, S.; Xu, B.; Ongoma, V.; Zhu, S.; Ma, H.; Li, X. Regional Features and Seasonality of Land–Atmosphere Coupling over Eastern China. *Adv. Atmos. Sci.* **2018**, *35*, 689–701. [CrossRef]

36. Hersbach, H.; Bell, B.; Berrisford, P.; Hirahara, S.; Horányi, A.; Muñoz-Sabater, J.; Nicolas, J.; Peubey, C.; Radu, R.; Schepers, D.; et al. The ERA5 Global Reanalysis. *Q. J. R. Meteorol. Soc.* **2020**, *146*, 1999–2049. [CrossRef]

37. Song, Y.; Wei, J. Diurnal Cycle of Summer Precipitation over the North China Plain and Associated Land–Atmosphere Interactions: Evaluation of ERA5 and MERRA-2. *Int. J. Climatol.* **2021**, *41*, 6031–6046. [CrossRef]

38. Sun, G.; Hu, Z.; Ma, Y.; Xie, Z.; Sun, F.; Wang, J.; Yang, S. Analysis of Local Land Atmosphere Coupling Characteristics over Tibetan Plateau in the Dry and Rainy Seasons Using Observational Data and ERA5. *Sci. Total Environ.* **2021**, *774*, 145138. [CrossRef]

39. Koster, R.D.; Guo, Z.; Dirmeyer, P.A.; Bonan, G.; Chan, E.; Cox, P.; Davies, H.; Gordon, C.T.; Kanae, S.; Kowalczyk, E.; et al. GLACE: The Global Land-Atmosphere Coupling Experiment. Part I: Overview. *J. Hydrometeorol.* **2006**, *7*, 590–610. [CrossRef]

40. Dirmeyer, P.A. The Terrestrial Segment of Soil Moisture-Climate Coupling. *Geophys. Res. Lett.* **2011**, *38*, L16702. [CrossRef]

41. Dirmeyer, P.A.; Wei, J.; Bosilovich, M.G.; Mocko, D. Intensified Land Surface Control on Boundary Layer Growth in a Changing Climate. *Geophysical* **2014**, *41*, 1290–1294. [CrossRef]

42. Hua, W.; Dong, X.; Liu, Q.; Zhou, L.; Chen, H.; Sun, S. High-Resolution WRF Simulation of Extreme Heat Events in Eastern China: Large Sensitivity to Land Surface Schemes. *Front. Earth Sci.* **2021**, *9*, 770826. [CrossRef]

43. Wei, J.; Su, H.; Yang, Z.L. Impact of Moisture Flux Convergence and Soil Moisture on Precipitation: A Case Study for the Southern United States with Implications for the Globe. *Clim. Dyn.* **2016**, *46*, 467–481. [CrossRef]

44. Santanello, J.A.; Peters-Lidard, C.D.; Kumar, S.V. Diagnosing the Sensitivity of Local Land-Atmosphere Coupling via the Soil Moisture-Boundary Layer Interaction. *J. Hydrometeorol.* **2011**, *12*, 766–786. [CrossRef]
45. Hirschi, M.; Seneviratne, S.I.; Alexandrov, V.; Boberg, F.; Boroneant, C.; Christensen, O.B.; Formayer, H.; Orlowsky, B.; Stepanek, P. Observational Evidence for Soil-Moisture Impact on Hot Extremes in Southeastern Europe. *Nat. Geosci.* **2011**, *4*, 17–21. [CrossRef]
46. Wu, L.Y.; Zhang, J.Y. Role of Land-Atmosphere Coupling in Summer Droughts and Floods over Eastern China for the 1998 and 1999 Cases. *Chin. Sci. Bull.* **2013**, *58*, 3978–3985. [CrossRef]
47. Schumacher, D.L.; Keune, J.; Dirmeyer, P.; Miralles, D.G. Drought Self-Propagation in Drylands Due to Land–Atmosphere Feedbacks. *Nat. Geosci.* **2022**, *15*, 262–268. [CrossRef] [PubMed]
48. Alessi, M.J.; Herrera, D.A.; Evans, C.P.; DeGaetano, A.T.; Ault, T.R. Soil Moisture Conditions Determine Land-Atmosphere Coupling and Drought Risk in the Northeastern United States. *J. Geophys. Res. Atmos.* **2022**, *127*, e2021JD034740. [CrossRef]
49. Cook, B.I.; Bonan, G.B.; Levis, S. Soil Moisture Feedbacks to Precipitation in Southern Africa. *J. Clim.* **2006**, *19*, 4198–4206. [CrossRef]
50. Samaniego, L.; Thober, S.; Kumar, R.; Wanders, N.; Rakovec, O.; Pan, M.; Zink, M.; Sheffield, J.; Wood, E.F.; Marx, A. Anthropogenic Warming Exacerbates European Soil Moisture Droughts. *Nat. Clim. Chang.* **2018**, *8*, 421–426. [CrossRef]
51. Zhou, S.; Williams, A.P.; Berg, A.M.; Cook, B.I.; Zhang, Y.; Hagemann, S.; Lorenz, R.; Seneviratne, S.I.; Gentine, P. Land–Atmosphere Feedbacks Exacerbate Concurrent Soil Drought and Atmospheric Aridity. *Proc. Natl. Acad. Sci. USA* **2019**, *116*, 18848–18853. [CrossRef] [PubMed]
52. Zhang, X.; Duan, Y.; Duan, J.; Jian, D.; Ma, Z. A Daily Drought Index Based on Evapotranspiration and Its Application in Regional Drought Analyses. *Sci. China Earth Sci.* **2022**, *65*, 317–336. [CrossRef]
53. Zhang, X.; Duan, J.; Cherubini, F.; Ma, Z. A Global Daily Evapotranspiration Deficit Index Dataset for Quantifying Drought Severity from 1979 to 2022. *Sci. Data* **2023**, *10*, 824. [CrossRef] [PubMed]
54. He, Q.; Lu, H.; Yang, K.; Leung, L.R.; Pan, M.; He, J.; Yao, P. A Simple Framework to Characterize Land Aridity Based on Surface Energy Partitioning Regimes. *Environ. Res. Lett.* **2022**, *17*, 34008. [CrossRef]